Available online at www.sciencedirect.com
ScienceDirect
Journal of Nuclear Materials 367–370 (2007) 915–919
journal of nuclear materials
www.elsevier.com/locate/jnucmat

A comprising steady-state creep model for the austenitic AISI 316 L(N) steel

Michael Rieth *

Forschungszentrum Karlsruhe, Institut für Materialforschung I, P.O. Box 3640, 76021 Karlsruhe, Germany

Abstract

Low-stress creep data of a recently finished special long-term program now allows for much better long-term predictions of the ITER related material 316 L(N) and also enables deformation modeling for a broader stress range. The present work focuses mainly on the set-up of a steady-state creep model with help of well-known rate-equations for different deformation mechanisms. In addition, the impact of microstructure changes and precipitation formation on steady-state creep is studied. The resulting creep model consists of a summation of contributions for diffusion creep, power-law creep, and power-law breakdown. The final creep model agrees well with experimental data for temperatures between 550 and 750 °C and for shear stresses above 30 MPa. The most important finding of this work is that for very low stresses the model predicts far higher creep rates than can be extrapolated from tests performed at the usual stress range of experimental programs.

1. Introduction

Among many other applications the 17/12/2-CrNiMo austenitic steel 316 L(N) (DIN 1.4909) is used or envisaged for both conventional and nuclear power plant construction as well as in the International Nuclear Fusion Project ITER. Worldwide, a huge number of experimental investigations have already been carried out to determine its creep properties in the conventional stress and temperature range [1–6].

In the design relevant low-stress range at 550 °C and 600 °C, however, creep data defining the stress dependence of the minimum creep rate or the technically relevant creep strain limits are almost unavailable. This is not only due to reasons of time, but to technical reasons, too. Therefore, a special long-term creep testing program at 550 °C and 600 °C was started in 1991 [7]. This low-stress creep data now allows for a much better long-term prediction of the reliability of 316 L(N) applications and also enables deformation modeling for a broader stress range.

2. Experimental details

Most data used in the current report result from experiments performed with heat No. 11477 from Creusot–Marell (CRM). This heat had been delivered as 40 mm hot rolled plate with a final heat treatment at 1100 °C followed by water quenching.

* Tel.: +49 7247 82 2909; fax: +49 7247 82 4567.
E-mail address: michael.rieth@imf.fzk.de

0022-3115/$ - see front matter © 2007 Elsevier B.V. All rights reserved.
doi:10.1016/j.jnucmat.2007.03.062

Quality assurance reported this batch as nearly free of δ-ferrite (<1%). In addition, some single data points have been taken from NRIM data sheets [6,8] for comparable alloys.

All creep specimens were produced out of the centre of the 40 mm plate (CRM 11477) transverse to the rolling direction. Loading took place in air via lever arms using weights. The continuously recorded strain curves have been digitalized and the creep rates have been obtained by numerical differentiation.

3. Microstructure

In the as delivered condition typical twin formations were recognizable as well as a slight texture along the rolling direction, combined with a few rather small inclusions. Other investigations have also shown small amounts of delta ferrite. After aging at 600 °C for 85000 h the microstructure has changed considerably. Precipitates have formed mainly at grain boundaries and along the rolling texture. A similar formation can be observed in SEM observations after 2650 h at 750 °C [9].

Sequence and types of precipitation in AISI 316 austenitic stainless steels are well-known [10,11]: $M_{23}C_6$ carbides are the first phases that form during aging where M represents Cr, Fe, Mo and Ni. Initially, these carbides consist of a higher amount of Fe that is usually replaced by Cr and/or Mo during aging. The most favorable precipitation sites are grain boundaries, followed by twins and dislocations where cold deformation enhances precipitation within grains. The presence of nitrogen inhibits or delays formation of $M_{23}C_6$ carbides. Therefore, at 600 °C with the present material $M_{23}C_6$ precipitation at grain boundaries starts after only a few hundred hours and the formation of carbides within grains takes 1000 h or more.

In addition to carbide precipitation, during long-term aging (especially at higher temperatures) AISI 316 steels are prone to formation of intermetallic phases. Below 800 °C usually $M_{23}C_6$ precipitation is followed by precipitation of Laves phase. In the case of the AISI 316 L(N) austenitic steel Laves phase consisting of Fe_2Mo starts to form after aging at 600 °C for about 10000 h, first at grain boundaries and finally within grains.

The last phase to appear is the sigma phase. It has very slow kinetics when forming from austenite and, therefore, takes aging of about 100000 h at 600 °C. But formation from ferrite is about 100 times faster. The composition of sigma phase in AISI 316 L(N) steels can be approximated by $(Fe, Ni)_3(Cr, Mo)_2$ or in wt%: 55Fe–29Cr–11Mo–5Ni. Sigma phase precipitates mainly on grain boundaries (especially on triple junctions) and on intragranular inclusions. A large amount of sigma phase precipitation finally leads to dendritic formations between and in some cases even within grains [9].

For an evaluation of the influence of the time-dependent microstructural composition on the creep behavior a precipitation diagram is necessary. At the National Institute for Materials Science, Japan extensive aging experiments have been performed followed by TEM examinations to generate a time–temperature-precipitation diagram for a 18Cr–12Ni–Mo steel that is comparable to the AISI 316 L(N) [12]. In Fig. 1 this precipitation map is shown together with the results of the 316 L(N) sigma phase observations. As can be seen, the results for both materials are in approximate agreement.

Now the question is: Can the steady-state creep rate be correlated with the aging (precipitation) behavior?

Looking at the high stress range, for example, shows only that, depending on temperature, there are none, some or even more carbide precipitation. But these do not reflect in the creep behavior. In the most interesting medium stress range there are either carbides at 550 °C or Laves phase precipitations at 600 °C. The same can be observed in the low-stress range at 650–750 °C. That is, neither $M_{23}C_6$ nor Laves phase precipitations can be the

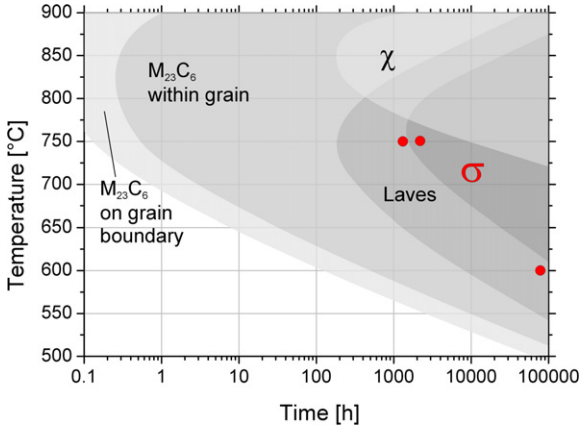

Fig. 1. Time–temperature-precipitation diagram by NIMS [15] for an austenitic stainless steel comparable to the AISI 316 L(N). The results of the AISI 316 L(N) sigma phase detection are shown as dots to demonstrate the agreement.

reason for a different creep rate behavior. Only the severe sigma phase formation could have had a significant influence on the creep properties. To check whether this is the case here, we have to correlate the steady-state periods with the times of sigma phase formation. But at times when sigma phase precipitation starts, the creep tests are already far away from minimum creep rates – even in the lowest stress range. Therefore, the change of microstructure with time has no influence on the steady-state creep in this case.

4. Creep model

Our model has been derived from four different well-known deformation mechanisms [13–20] which are described by rate equations.

4.1. Diffusion creep

For the description of diffusion creep we use [14–19] where the creep rate $\dot{\gamma}_{sC}$ is given by:

$$\dot{\gamma}_{sC} = 42\ \Omega \frac{1}{d^2}\frac{\sigma_s}{kT}\left(D_L + \frac{\pi\delta}{d}D_B\right), \tag{1}$$

where D_L and D_B are lattice and boundary diffusion coefficients [13], respectively, with

$$D_L = D_{0L}e^{-\frac{Q_L}{RT}} \quad \text{and} \quad D_B = D_{0B}e^{-\frac{Q_B}{RT}}. \tag{2}$$

In this model most constants are well-known, like the atomic volume Ω, grain size d, and grain boundary thickness δ (see Table 1). Since boundary diffusion data are not readily available for the present material the values have to be determined from the experiments and reasonable assumptions. In our case the boundary diffusion activation energy Q_B has been chosen to be 200 kJ/mol which is about 20% higher than the value reported for 316 steels [12]. With this, the assumption that the contributions of lattice and boundary diffusion are equal at about 0.6 T_M leads to a value for D_{0B} of $6 \cdot 10^{-6}$ m^2/s.

Only the long-term creep tests performed at 600 °C are near the range dominated by boundary diffusion creep. According to our model, all other tests have not been influenced by diffusion creep. Lattice diffusion certainly plays no role for the given temperature range. Its contribution to the strain rate becomes relevant only at much higher temperatures (>0.6 T_M) where it dominates over the contribution of grain boundary creep.

Table 1
Diffusion creep, plasticity, power-law and power-law break-down parameters used for the AISI 316 L(N) stainless steel

Parameter	Value
Lattice diffusion coefficient, D_{0L}	37.5×10^{-6} m^2/s
Lattice diffusion activation energy, Q_L	280 kJ/mol
Boundary diffusion coefficient, D_{0B}	6×10^{-6} m^2/s
Boundary diffusion activation energy, Q_B	200 kJ/mol
Activation energy, Q_P	460 kJ/mol
Activation energy, ΔF	1.04×10^{-18} J
Obstacle spacing, l	40 nm
Pre-exponential, $\dot{\gamma}_0$	10^6 1/s
Pre-constant, c_3	2×10^{20}
Core diffusion coefficient, D_{0C}	10×10^{-6} m^2/s
Core diff. activation energy, Q_C	520 kJ/mol
Creep exponent, n	5
Constant, α'	800

4.2. Plasticity (Dislocation glide)

Low-temperature plasticity is a high stress deformation mechanism. Therefore, it plays only a minor role in creep. However, to cover the whole stress range in our model we use the simplified description for plasticity [13] which reads

$$\dot{\gamma}_{sP} = \dot{\gamma}_0\ \exp\left[-\frac{\Delta F}{kT}\left(1 - \frac{\sigma_s}{\hat{\tau}}\right)\right] \quad \text{or}$$

$$\dot{\gamma}_{sP} = \dot{\gamma}_0 \exp\left[-\frac{Q_P}{RT}\left(1 - \frac{\sigma_s}{\hat{\tau}}\right)\right] \tag{3}$$

For the present material $\hat{\tau}$ can be approximated as

$$\hat{\tau} \approx \frac{\mu b}{l}, \tag{4}$$

where b is the magnitude of Burgers' vector, l is the obstacle and/or solute spacing parameter (in this context obstacles may be dispersions, precipitates, forest dislocations, lattice resistance, solutes, etc), and μ is the temperature dependent shear modulus given by

$$\mu = \mu(T) = \mu_0\left(1 - 0.85\frac{T - 300\ K}{T_M}\right). \tag{5}$$

In [13] $\frac{\hat{\tau}}{\mu} \approx 6.5 \cdot 10^{-3}$ is given for 316 stainless steel. With that the spacing parameter l takes a value of about 40 nm. The activation energy ΔF has been estimated to be about 0.75 $\mu_0 b^3$ which correspond to $Q_P = 460$ kJ/mol.

4.3. Power-law creep (dislocation climb)

Usually, power-law creep includes dislocation climb, activated by lattice and core diffusion [21].

But as has been demonstrated with the diffusion creep model (Section 4.1), lattice diffusion can be completely neglected within the present temperature range. Therefore, the expression for power-law creep reduces to

$$\dot{\gamma}_{\mathrm{sPL}} = c_3 \frac{\mu b}{kT} \left(\frac{\sigma_s}{\mu}\right)^{n+2} D_C, \tag{6}$$

where D_C is the core diffusion coefficient with

$$D_C = D_{0C}\, e^{-\frac{Q_C}{RT}}. \tag{7}$$

D_C is of the same order of magnitude as the grain boundary diffusion constant D_B and has therefore been chosen to be 10^{-5} m^2/s. Again, the shear modulus μ depends on temperature as given in Eq. (5).

This leaves three remaining parameters – the exponent n, the activation energy Q_C, and the constant c_3 – which have to be fitted to the experimental data. In log–log-representation the slope is defined by n, the vertical distance by Q_c, and the offset by c_3. Here the parameters have been chosen as follows: $Q_C = 520$ kJ/mol, $n = 5$, and $c_3 = 2 \cdot 10^{20}$.

4.4. Transition from creep by climb to creep by glide

At stresses above about $10^{-3}\,\mu$ the power-law breaks down [16]. That is, starting from this point (for the present material the onset is at 86 MPa) the model has to describe a transition from creep by climb (power-law) to creep by glide (plasticity).

In our model this is expressed by

$$\dot{\gamma}_{\mathrm{sPLBD}} = c_3 \left[\sinh\left(\alpha' \frac{\sigma_s}{\mu}\right)\right]^{n+2} D_C \tag{8}$$

which leaves only one free parameter (α') to fit to experiment. For this we have only used data from the 600 °C creep tests to verify the result later on with the other data and we have chosen $\alpha' = 800$.

5. Discussion

To obtain the complete model all contributions have to be summed up accordingly:

$$\dot{\gamma}_s = \dot{\gamma}_{sC} + \dot{\gamma}_{sP} + \begin{cases} \dot{\gamma}_{\mathrm{sPL}} & \text{for } \sigma_s \leqslant 86\ \mathrm{MPa} \\ \dot{\gamma}_{\mathrm{sPLBD}} & \text{for } \sigma_s > 86\ \mathrm{MPa} \end{cases} \tag{9}$$

where the single contributions are given by the Eqs. (1), (3), (6), and (8). A comparison of the model predictions and the experimental data is given in Fig. 2.

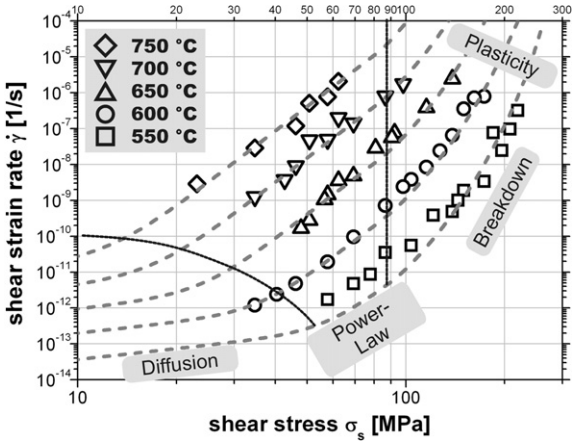

Fig. 2. Creep model (dashed lines) compared to the experimental results (symbols). The regimes of dominant deformation mechanisms are approximated (dotted lines).

The transition from power-law creep to plasticity (which has been fitted to the 600 °C results) also fits nicely to the results obtained at 550 and 650 °C. At higher temperatures the experiments have been performed at stresses below the transition range.

The power-law creep range which has been fitted to the 600, 650 and 700 °C results, applies also for the 750 °C tests. The experiments at 550 °C, however, are well above the predictions from the model.

Only the creep tests performed at 600 °C reach the range of diffusion creep. Therefore, it is not possible to verify the model for the other temperatures. But, at least for 600 °C, the model predictions perfectly fit the experiments.

To adapt the model to creep experiments with the AISI 316 L(N) steel only a few parameters are needed:

- grain boundary diffusion coefficient and activation energy to describe diffusion creep,
- a generic constant, the core diffusion coefficient and activation energy, and the power exponent to describe power-law creep,
- and a generic constant for the description of the transition from power-law creep to plasticity.

To determine all parameters from experimental data, it requires creep tests at three different temperatures in the usual stress range and at least some long-term experiments which reach into the diffusion creep regime. In the present case the latter was not quite fulfilled. Therefore, diffusion creep might be described somewhat too conservative. However, all data (with the exception of the

550 °C long-term experiments) fit nicely to the model predictions. But these experiments were probably aborted too soon, that is, it was not possible to extract reliable minimum creep rates.

6. Conclusions

It has been demonstrated that for a description of the steady-state creep behavior of type 316 L(N) stainless steel, only grain boundary diffusion, power-law creep, and the transition from dislocation climb to dislocation glide are relevant, where the latter is just a limit that is barely reached with constant load creep tests. This led to a model consisting of three main deformation mechanisms and two transitions:

- At very low-stresses only grain boundary diffusion contributes to the strain rate which is proportional to the stress ($\sim\sigma$). This regime can only be reached by performing extremely long-term tests. In the present case there are indications that diffusion creep occurred after 10 years at 600 °C.
- Then there is a relatively sharp transition to creep triggered by dislocation climb. In the present case, dislocation climb depends on core diffusion and leads to creep rates proportional to the 7th power of stress ($\sim\sigma^7$) – thus the name *Power-law creep*.
- Starting from medium stresses there is a continuous transition from creep by dislocation climb to plasticity which depends solely on dislocation glide. The plasticity regime is usually not reached in creep tests. Here the strain rate depends exponentially on stress ($\sim e^{\sigma}$).

Acknowledgement

This work was performed within the framework of the FUSION Project of Forschungszentrum Karlsruhe.

References

[1] T. Nakazawa, Mater. Sci. Eng. A 148 (1988) 253.
[2] M.D. Mathew, International Conference on High Nitrogen Steels, HNS 88, Lille, France, 18–20 May, 1988.
[3] M. Schirra, Nucl. Eng. Design 147 (1993) 63.
[4] M. Schirra, Nucl. Eng. Design 188 (1999) 381.
[5] M. Schirra, KfK-Reports 4767, 4861, and 6699, Forschungszentrum Karlsruhe, Germany, September 1990, August 1991 and February 2002.
[6] NRIM-Creep Data Sheet No. 42-1996, National Research Institute for Metals, Tokyo, Japan.
[7] M. Schirra, Annual Meeting on Nuclear Technology, Aachen, Germany, 13–15. May 1997.
[8] NRIM-Creep Data Sheets No. 14A-1982, 15A-1982, 45-1997 and 6B-2000, National Research Institute for Metals, Tokyo, Japan.
[9] A.F. Padilha, D.M. Escriba, E. Materna-Morris, M. Rieth, M. Klimenkov, J. Nucl. Mater. (2006), doi:10.1016/j.jnucmat.2006.12.027.
[10] A.F. Padilha, P.R. Rios, ISIJ Int. 42 (2002) 325.
[11] P.R. Rios, A.F. Padilha, in: K.H. Buschow et al. (Eds.), Encyclopedia of Materials: Science and Technology, Elsevier, Amsterdam, 2001, p. 7836.
[12] NRIM-Metallographic Atlas of Long-term Crept Materials No. M-2, National Research Institute for Metals, Tokyo, Japan, 2003.
[13] H.J. Frost, M.F. Ashby, Deformation-mechanism Maps, Pergamon, Oxford, 1982.
[14] F.R.N. Nabarro, in: Report on Conference on Strength of Solids, Phys. Soc. London, 75, 1948.
[15] C. Herring, J. Appl. Phys. 21 (1950) 437.
[16] F. Garofalo, Fundamentals of Creep and Creep-Rupture in Metals, MacMillan, New York, 1965.
[17] B. Chalmers, Physical Metallurgy, John Wiley, New York, 1959.
[18] A.P. Greenough, Philos. Mag. 43 (1953) 1075.
[19] B.H. Alexander, M.H. Dawson, H.P. Kling, J. Appl. Phys. 22 (1951) 439.
[20] J. Weertman, J. Mech. Phys. Solids 4 (1956) 230;
J. Weertman, Trans. AIME 218 (1960) 207;
J. Weertman, Trans. AIME 227 (1963) 1475.
[21] L.D. Blackburn, The Generation of Isochronous Stress-Strain Curves, in: ASME Winter Annual Meeting, New York, 1972.